Shallow storage conditions at Krafla IDDP-1 revealed by rhyolite-MELTS geobarometry, and implications for global shallow magmatism

Lydia J. Harmon,[a] * Guilherme A. R. Gualda,[a] Blake M. Wallrich,[a] Calvin F. Miller[a]

[a]Vanderbilt University, Department of Earth & Environmental Sciences, 2301 Vanderbilt Place, Nashville, TN 37235

* Corresponding author: harmonl@oxy.edu

Abstract

Identifying the storage depths of melt-dominated magma bodies prior to eruption is critical for understanding magma transport, eruption hazards, and magma body longevity. Rhyolite-MELTS has been used effectively to calculate pre-eruptive storage pressures for silicic magma bodies in the upper crust (~100-350 MPa), but its precision and accuracy in very low-pressure systems (<100 MPa) has not been sufficiently investigated. During the recent Krafla IDDP-1 drilling project, magma was surprisingly intersected at 2.1 km depth. Here, we test the use of rhyolite-MELTS geobarometry for this very low-pressure system, using natural Krafla IDDP-1 compositions that were stored at a known depth. We input the composition of the melt (preserved as glass) and search in pressure and temperature space at a range of oxygen fugacity (f_{O2}) to model the storage conditions of the Krafla magma. For the average composition of the drilled melt, rhyolite-MELTS yields reasonable storage pressures (~40-50 MPa). After converting calculated pressure to depth, the calculated depths are 1.6-1.9 km. These estimates are only 0.2-0.5 km different from that of the intersected magma, showing that rhyolite-MELTS provides excellent estimates for very shallow magma storage, further strengthened by results from a Monte Carlo analysis. The agreement between rhyolite-MELTS pressures and the drilled depth of the Krafla magma supports the previously calculated very shallow storage pressures in other locations, like the Taupō Volcanic Zone (TVZ), Aotearoa New Zealand. This shallowest storage zone of melt-dominated magmas has significant implications for modeling volcanic unrest and evaluating geothermal and economic resource potential.

Keywords

Shallow magma, rhyolite-MELTS, geobarometry, Krafla

Introduction

Motivation

Rhyolitic magmas are integral to the formation and differentiation of the crust, especially of the upper crust. They often erupt explosively and are responsible for some of the largest eruptions on record (Lowenstern *et al.*, 2006; Self, 2006; Miller and Wark, 2008). Identifying where melt-dominated magma bodies of rhyolite form and are stored in the crust is critical for understanding magma body generation and longevity (Gualda *et al.*, 2012b; Pamukçu *et al.*, 2015a, 2021; Till *et al.*, 2015; Bachmann and Huber, 2016; Townsend and Huber, 2020), magma decompression and ascent (Putirka, 2016a; Polacci *et al.*, 2017; Cassidy *et al.*, 2018; Caricchi *et al.*, 2021), and eruption hazards (Tilling, 2008; Aspinall and Blong, 2015; Cassidy and Mani, 2022).

Substantial effort and progress have been made to determine the depths of pre-eruptive magma storage via erupted products using a variety of methods, for instance: clinopyroxene and amphibole geobarometry (Blundy and Holland, 1990; Thomas and Ernst, 1990; Schmidt, 1992; Nimis and Ulmer, 1998; Putirka et al., 2003; Putirka, 2008, 2016b; Mutch et al., 2016; Neave and Putirka, 2017; Petrelli et al., 2020; Jorgenson et al., 2022; Wieser et al., 2022, 2023), fluid-inclusion geobarometry (Moore, 2008; Wallace *et al.*, 1999; Anderson *et al.*, 2000) , and field work in volcanic-plutonic systems (Hogan and Gilbert, 1995; du Bray and Pallister, 1999; Bachl *et al.*, 2001; Ferguson *et al.*, 2013; Deering *et al.*, 2016; Chen *et al.*, 2021; Wallrich *et al.*, 2023). As well, indirect observations document magma and magma bodies via geophysical methods (Lees, 2007; Lerner *et al.*, 2020; Paulatto *et al.*, 2022).

Pre-eruptive magma storage depths of rhyolites are typically considered to be ≥ 3 km, with the depth of 5-10 km commonly considered the dominant depth range of upper crustal magmas that feed eruptions to the surface (Cashman and Giordano, 2014; Cashman *et al.*, 2017; Tramontano *et al.*, 2017; Huber *et al.*, 2019). However, there are also multiple examples of inferred present-day shallow magma storage, at depths < 3 km, for instance: Larderello geothermal field, Italy (Cameli *et al.*, 1993; Manzella *et al.*, 2017; Rochira *et al.*, 2018) and Dabbahu volcano, Afar, Ethiopia (Wright *et al.*, 2006; Ebinger *et al.*, 2008). Several instances where magma has been directly intersected at much shallower depths via drilling document unequivocally the existence of very shallow silicic magma storage. They are: 1) Puna Geothermal field, Hawai'i at 2.5 km in 2005 (Teplow *et al.*, 2009); 2) Menengai Caldera, Kenya at 2.1 km and 2.2 km in 2011-2014 from well MW-04 and MW-06 (Mbia *et al.*, 2015); and 3) Krafla geothermal system, Iceland at 2.6 km in 2008 from well KJ-39 in the Suðurhlíðar well field (Mortensen *et al.*, 2010) and at 2.1 km in 2009 from the Krafla IDDP-1 well (Elders *et al.*, 2011; Zierenberg *et al.*, 2013).

Thermodynamic phase-equilibria modeling via rhyolite-MELTS has been utilized to determine pre-eruptive storage conditions, including depth and f_{O2}, in predominantly silicic systems (Gualda *et al.*, 2012a; Bégué *et al.*, 2014b; Gualda and Ghiorso, 2014; Pamukçu *et al.*, 2015b; Harmon *et al.*, 2018). Here, we investigate the efficacy of rhyolite-MELTS geobarometry to infer the presence of very shallow magma bodies. Krafla IDDP-1 glass compositions provide a natural laboratory to test the validity and sensitivity of this approach for evaluating shallow storage depths of silicic magmas.

Krafla

The Krafla central volcano is located within the Northern Rift Zone of Iceland. Krafla has erupted predominantly basalt throughout its ~300 ka volcanic history (Thorarinsson, 1979; Sæmundsson, 1991), and there have been at least 8 rhyolitic eruptions (Sæmundsson, 1991; Jonasson, 1994; Rooyakkers *et al.*, 2021). The Krafla caldera collapsed at ~110 ka (Calderone *et al.*, 1990; Sæmundsson and Pringle, 2000; Rooyakkers *et al.*, 2019), and the modern-day geothermal field is located within this caldera structure. The most recent eruption is the Krafla Fires, which continued intermittently from 1975 to 1984, and did not contain rhyolite (Einarsson, 1978; Hollingsworth *et al.*, 2012). The most recent rhyolitic eruption, the 1724 C.E. Mývatn Fires rifting episode that formed the Víti maar is compositionally similar to the IDDP-1 glass studied here. These compositions are distinct form previous rhyolitic eruption from Krafla (Rooyyakers et al., 2021)

There has been substantial geothermal exploration since 1974, which has revealed extensive active geothermal systems and refined the understanding of the subsurface geology (Árnadóttir *et al.*, 1998; Árnason *et al.*, 2008; Kennedy *et al.*, 2018, 2018b; Árnason, 2020).

In 2009, during the IDDP drilling project, the IDDP-1 well was designed to drill to 4-5 km depth (Frioleifsson *et al.*, 2014), but surprisingly intercepted magma at 2.1 km, despite substantial seismic and subsurface imaging (Elders *et al.*, 2011). Quenched glass fragments were recovered in the drill cuttings and allow observation and analysis of magma intercepted at depth (Elders *et al.*, 2011; Zierenberg *et al.*, 2013; Masotta *et al.*, 2018). The magma is rhyolitic (~76.1-77.3 wt%

SiO_2) with ~1.8 wt% dissolved volatiles of mixed H_2O-CO_2 (Elders *et al.*, 2011), suggesting saturation pressures of ~40 MPa (Zierenberg *et al.*, 2013). Intersected rhyolite was in contact with a felsite host (Elders *et al.*, 2011; Zierenberg *et al.*, 2013; Masotta *et al.*, 2018). Isotopically, the magma is likely formed from melting hydrothermally altered basalt as opposed to forming via fractional crystallization (Elders *et al.*, 2011; Zierenberg *et al.*, 2013; Kennedy *et al.*, 2018).

Previous work on the IDDP-1 drill cuttings includes major-element glass analyses, bubble texture analyses, and experimental studies (Elders *et al.*, 2011; Zierenberg *et al.*, 2013; Masotta *et al.*, 2018; Rooyakkers *et al.*, 2021; Saubin *et al.*, 2021). We point the reader to several excellent studies for further information, including: Elders *et al.* (2011), Saubin *et al.* (2021), Zierenberg *et al.* (2013), and Masotta *et al.* (2018).

Rhyolite-MELTS

Rhyolite-MELTS is an internally consistent phase-equilibria thermodynamic model. We utilize rhyolite-MELTS to determine the magmatic conditions at which a melt of a given composition is in equilibrium with a known/observed mineral assemblage (Gualda *et al.*, 2012a; Bégué *et al.*, 2014b; Gualda and Ghiorso, 2014; Pamukçu *et al.*, 2015b; Harmon *et al.*, 2018, 2024; Smithies *et al.*, 2023). We use the composition of natural volcanic glass from Krafla as a proxy for the magmatic melt, and we search for the conditions at which melt of the given composition is in equilibrium with an expected mineral assemblage. The pressure calculated by rhyolite-MELTS is the pressure at which the melt was last in equilibrium with the mineral assemblage, which is interpreted to be the pre-eruptive magma storage pressure. This is particularly appropriate for Krafla IDDP-1 magmas, given that they were sampled at depth, without any effects of ascent and eruption.

Rhyolite-MELTS geobarometry has been applied to a variety of volcanic systems (Gualda and Ghiorso, 2013a; Bégué *et al.*, 2014b; Gualda *et al.*, 2018; Foley *et al.*, 2020; Pamukçu *et al.*, 2021; Pitcher *et al.*, 2021; Seropian *et al.*, 2021; Smithies *et al.*, 2023; Harmon *et al.*, 2024). For the most part, these studies have shown that pre-eruptive storage predominately takes place under pressures of ~100-300 MPa. Nonetheless, work focusing on the Taupō Volcanic Zone (TVZ) has revealed a subset of rhyolite-MELTS pressures of ~50-75 MPa (Bégué *et al.*, 2014b, 2014a; Gualda *et al.*, 2018; Pamukçu *et al.*, 2020; Harmon *et al.*, 2024). Because such shallow pressures were not as well constrained as others (see Bégué *et al.*, 2014b), these results – and their potential significance – have not been the focus of any of these studies. However, the existence of these very shallow pre-eruptive magma storage pressures (<100 MPa) hint that 1) there is a very shallow depth of pre-eruptive magma storage that has been relatively unexplored; and 2) rhyolite-MELTS has the potential to resolve very shallow magma storage.

The well-studied Krafla system provides an opportunity to test the efficacy and precision of rhyolite-MELTS storage pressures for very shallow magma bodies, given that magma depth is known. Confirmation of rhyolite-MELTS pressures in the Krafla IDDP-1 case study would lend support to very shallow pressures indicated elsewhere in the world, with potentially important implications for our understanding of the architecture of magmatic systems that feed eruptions to the surface.

Materials and Methods

Krafla Glass Compositions

We use the 31 natural quenched rhyolite glass compositions from Masotta *et al.* (2018) for Krafla IDDP-1 magmas, and we also calculate an average composition based on these 31 compositions. These compositions are the rhyolite (“RHL”) compositions from Masotta *et al.* (2018), which are most similar to the Melt 1 compositions reported by Zierenberg *et al.* (2013), interpreted to be generated by partial melting at depth (much deeper than the depth of intersection) of a hydrothermally altered basaltic crust (Zierenberg *et al.*, 2013). We take these RHL compositions from Masotta *et al.* (2018) to be best estimates of Krafla melt compositions, and we use them as input for rhyolite-MELTS calculations (see supplementary data for compositions). The compositions are retrieved from mm-sized glass pieces that rapidly quenched during interaction with the drilling fluids. The observed mineral assemblage in the mm-sized shards is plagioclase + augite + pigeonite + magnetite ± apatite (Zierenberg *et al.*, 2013; Masotta *et al.*, 2018), and the samples have <3% crystals (Zierenberg *et al.*, 2013). Volatile contents measured using FTIR yield average total H_2O content of ~ 1.8 wt% and CO_2 content of ~ 85 ppm (Zierenberg *et al.*, 2013). Directly adjacent to the melt-rich magma body was a partially melted felsite with a mineralogy of plagioclase + alkali feldspar + quartz + augite + magnetite + zircon ± apatite (Elders *et al.*, 2011; Zierenberg *et al.*, 2013).

While there has not been a direct estimate of the f_{O2} for the magma intersected by the IDDP-1 drilling, the f_{O2} conditions of Krafla basalts have been calculated to be at the QFM buffer

(Nicholson, 1990) or just above it (ΔQFM = +0.6-0.7) (Shorttle *et al.*, 2015; Hartley *et al.*, 2017; Halldórsson *et al.*, 2018), which is ~1 log unit below the NNO buffer (ΔNNO = -1).

Projection onto the Haplogranitic Ternary Diagram

We project all Krafla IDDP-1 compositions onto the quartz-albite-orthoclase haplogranitic ternary using the projection scheme of Blundy and Cashman (2001), which yields a first order estimate of crystallization pressures for melts in equilibrium with quartz and feldspar (Gualda and Ghiorso, 2013b). For magmas in which quartz is absent, such as Krafla magmas, pressures obtained with this projection represent maximum pressures of magma storage.

For comparison, we also project all TVZ compositions that produced pressures ≤ 100 MPa from Bégué *et al.* (2014) and Gualda *et al.* (2018) onto the haplogranitic ternary. In this case, quartz is generally observed, which suggests that projection onto the haplogranitic ternary yields best-estimates of storage pressures.

Rhyolite-MELTS Calculations

Rhyolite-MELTS geobarometry yields the pressures at which the input glass composition (the best proxy for the magmatic melt composition) was last in equilibrium with the mineral assemblage. We use MELTS_Excel (Gualda and Ghiorso, 2015), following the methods detailed in Gualda and Ghiorso (2014) for all pressure calculations. The inputs for rhyolite-MELTS are the compositions of the quenched rhyolite glass retrieved from the Krafla IDDP-1 drilling (Masotta *et al.*, 2018). Rhyolite-MELTS is not given any other information a priori, including the mineral phases of interest. We search through pressure, temperature, and f_{O2} space.

The ranges of pressure (200-10 MPa in 10 MPa steps), temperature (1100-700 °C in 1 °C steps), and f_{O2} (ΔNNO = -3, -2.5, -2, -1.5, -1.25, -1, -0.75, -0.5, and 0) were chosen to explore very shallow storage pressures, from above the liquidus to near-solidus temperatures, and over the possible range of f_{O2} expected for the system (Elders *et al.*, 2011; Zierenberg *et al.*, 2013). We run all compositions at fluid saturated conditions, using a pure-H_2O fluid model. At such shallow conditions, the Krafla magma is likely fluid saturated (Zierenberg *et al.*, 2013). Gualda and Ghiorso (2014) (2014) and Ghiorso and Gualda (2015) demonstrate that water has a small effect on calculated pressures for magmas that are rich in water.

Rhyolite-MELTS models the saturation surfaces of solid phases in equilibrium with the given melt composition. For the Krafla IDDP-1 compositions, phases that rhyolite-MELTS predicts to be possibly saturated under the conditions considered include quartz, plagioclase (labeled as feldspar1 in MELTS_Excel results), orthopyroxene, and magnetite (labeled as spinel in MELTS_Excel results); clinopyroxene is not predicted to be potentially saturated. The saturation surfaces of quartz and feldspar are not sensitive to f_{O2}, in contrast to the saturation surfaces of orthopyroxene and magnetite, due to the presence of iron in orthopyroxene and magnetite. Therefore, pressure calculations that include orthopyroxene and, particularly, magnetite are highly dependent on f_{O2}, which allows us to estimate f_{O2} in addition to pressure (Harmon *et al.*, 2018; Pamukçu *et al.*, 2021). The differences between the observed and modeled mineral assemblages are discussed in further detail in the Discussion section.

Following Foley *et al.* (2020) and Gualda et al. (XX in revision), we extend the methods of Gualda and Ghiorso (2014) and Harmon *et al.* (2018) to calculate equilibrium pressures of the simultaneous saturation in quartz, plagioclase, orthopyroxene, and magnetite (which we label P_4 QFOM). We also calculate pressures based on the simultaneous saturation in quartz, plagioclase, and orthopyroxene (P_3 QFO); and based on the simultaneous saturation in quartz, plagioclase, and magnetite (P_3 QFM). We note that all three conditions (P_4 QFOM, P_3 QFO, and P_3 QFM) imply saturation in quartz and plagioclase, which are independent of f_{O2}.

For P_4 QFOM pressures, we calculate a pressure when the residual temperature (the minimum range in saturation temperature for all phases at a single pressure, calculated by subtracting the saturation temperatures of the mineral phase with the highest saturation temperature from the mineral phase with the lowest saturation temperature at a single pressure) is less than 10 °C (Figure 1). If no acceptable P_4 QFOM pressure is found, we calculate P_3 QFM and P_3 QFO pressures if the residual temperature is less than or equal to 5 °C, as in Gualda and Ghiorso (2014). The larger residual cutoff for P_4 QFOM is used due to uncertainties inherent in the exercise of finding an intersection between 4 saturation surfaces, particularly when two of them are affected by f_{O2}.

To convert the calculated pressures to depths, we use $h = P/(\rho * g)$ where h is the depth (m), ρ is the density of the crust (estimated to be 2,500-2,700 kg/m^3), P is the calculated pressure (Pa), and g is the acceleration due to gravity (9.8 m/s^2). We report the depths in units of km, so that we do not overinterpret the precision of the rhyolite-MELTS results. This represents the lithostatic pressure, which is a maximum depth assuming no hydrostatic component of the system.

Monte Carlo Analysis

To determine the reproducibility, variability, and precision of the rhyolite-MELTS pressure and f_{O2} estimates, we conduct a Monte Carlo analysis (Gualda and Ghiorso, 2014; Pamukçu *et al.*, 2021; Pitcher *et al.*, 2021; Smithies *et al.*, 2023) using 600 synthetic glass compositions based on the average Krafla composition and uncertainty around this composition. The f_{O2} was allowed to vary in 0.5 ΔNNO steps from ΔNNO = -3 to 0. The rhyolite-MELTS calculations in the Monte Carlo simulations explore the same pressure and temperature ranges detailed above.

Results

Projection onto the Haplogranitic Ternary Diagram

The average Krafla rhyolite composition plots approximately on the 50 MPa cotectic curve in the Qz'-Ab'-Or' ternary diagram (Figure 2). Individual compositions have values that range from just above the 50 MPa cotectic (i.e, shifted towards the Qz' vertex) to just below the 100 MPa cotectic (i.e., shifted towards the Ab'-Or' join). These results correspond to maximum pressures that range from slightly less than 50 MPa to slightly more than 100 MPa. The haplogranitic Qz'-Ab'-Or' ternary gives a first order estimate of the equilibration pressures. We emphasize that the absence of quartz simply imply that pressures should be lower than estimated from the diagram, suggesting that Krafla magmas equilibrated at very low pressures, most likely <50 MPa.

As originally observed by Bégué *et al*. (2014a), when plotted on the Qz'-Ab'-Or' ternary diagram, TVZ compositions that yield the lowest pressures exhibit low pressures (~50-150 MPa), but which are slightly higher than Krafla IDDP-1 pressures. The TVZ samples all contain quartz, indicating that these pressures can be unambiguously interpreted to be storage pressures.

Rhyolite-MELTS Pressures

A total of 26 of the 31 individual RHL Krafla compositions (84%) yield pressures for at least one of the nine f_{O2} values we explored. Results from individual Krafla compositions are summarized in Table 1 and Figure 3. A total of 143 of the 279 rhyolite-MELTS runs (51%) yield storage pressures. Individual compositions can yield more than one pressure in the cases in which pressures are calculated for multiple f_{O2} values.

Individual compositions return P_4 QFOM pressures for f_{O2} values of Δ NNO = -1 to -0.5, with the most pressure calculations confined to the even narrower f_{O2} range of Δ NNO = -1 and -0.75. The average pressure for all P_4 QFOM pressures (regardless of f_{O2}) is 50 ± 11 MPa (1-sigma), which corresponds to a depth of 1.9-2.0 ± 0.4 km.

For more reducing conditions (f_{O2} equal to ΔNNO = -3 to -1), individual compositions return predominantly P_3 QFO pressures. A total of 117/279 (42%) of the rhyolite-MELTS runs return P_3 QFO pressures. The average pressure for all P_3 QFO pressures (regardless of f_{O2}) is 44 MPa ± 11 MPa (1.7-1.8 km ± 0.4 km).

For more oxidizing conditions (f_{O2} equal to ΔNNO = -1 to 0), individual compositions return predominantly P_3 QFM pressures. A total of 46/279 (16%) of the rhyolite-MELTS runs return P_3 QFM pressures. The average pressure for all P_3 QFM pressures (regardless of f_{O2}) is 47 MPa ± 32 MPa (1.8-1.9 km ± 1.2-1.3 km).

The average Krafla IDDP-1 composition returns a P_4 QFOM pressure of 42 MPa (1.6-1.7 km) for ΔNNO = -0.75 and 46 MPa (1.7-1.9 km) for ΔNNO = -1. These are the only f_{O2} values that return a P_4 QFOM pressure for the average Krafla IDDP-1 composition, indicating that – as expected – the calculations of storage pressure using four phases are highly dependent on f_{O2}. The sensitivity of the rhyolite-MELTS calculations to f_{O2}, temperature, and pressure are highlighted in Figure 4, where there is only a small "valley" in the average composition data that produces P_4 QFOM pressures. We highlight the average Krafla calculations, but the shape of the surface in Figure 4 is similar for all individual rhyolite-MELTS calculations.

Only a narrow range of f_{O2} values produce P_4 QFOM pressures. The P_3 QFM and P_3 QFO pressures show somewhat larger ranges of pressure and f_{O2} (Figures 3 and 4). The overall distribution of pressures is similar for all assemblages and f_{O2} values.

Monte Carlo Simulations

Results from the Monte Carlo simulations are summarized in Figure 5 and Table 2. A total of 373/600 (62%) of rhyolite-MELTS runs return a valid pressure. The phase assemblages considered are the same assemblages considered for the individual compositions (P_4 QFOM, P_3 QFO, and P_3 QFM). There are 27 compositions (5%) that return P_QFOM pressures. The f_{O2} values that produced these P_4 QFOM pressures are equal to ΔNNO = -1 (20 compositions) and -0.5 (7 compositions). The average pressure for all P_4 QFOM pressures (regardless of f_{O2}) is 48 MPa ± 8 MPa, which corresponds to a depth of 1.8-2.0 km ± 0.3 km assuming lithostatic pressure.

There are 317/600 compositions (53%) that return P_3 QFO pressures and 83 compositions (14%) return P_3 QFM pressures. The average pressure for all P_3 QFO pressures (regardless of f_{O2}) is 46 MPa ± 20 MPa (1.7-1.9 km ± 0.8 km) and the average pressure for all P_3 QFM pressures (regardless of f_{O2}) is 37 MPa ± 13 MPa (1.4-1.5 km ± 0.5 km). A similar trend to the individual compositions is observed, as P_3 QFO pressures are calculated for more reducing conditions and P_3 QFM pressures are calculated for more oxidizing conditions for the Monte Carlo results.

Discussion

Hydrostatic vs lithostatic pressures

The quenched glass fragments retrieved from 2.1 km depth at the Krafla IDDP-1 well allow us to test the reliability of rhyolite-MELTS pressures for very low pressures (~50 MPa), with important implications for our understanding of magma storage conditions. While the depth of the magma intersected by Krafla IDDP-1 is known, determining the *in situ* pressure conditions experienced by the magma is more nuanced. The bounds of acceptable pressures are defined by the lithostatic pressure and by the hydrostatic pressure. The lithostatic pressure for this magma at 2.1 km is ~51-56 MPa using a rock density of 2,500-2,700 kg/m^3. In contrast, the hydrostatic pressure is calculated to be ~16 MPa (Zierenberg *et al.*, 2013). Based on H_2O and CO_2 concentrations in glass determined with FTIR, Zierenberg et al. (2013) calculate an H_2O-CO_2 saturation pressure of ~35-45 MPa using VolatileCalc and assuming a temperature of 900 °C (Newman and Lowenstern, 2002). Rhyolite-MELTS calculations return pressures between lithostatic and the H_2O-CO_2 saturation pressure, suggesting that the Krafla magma body was nearly fluid saturated, but possibly at a pressure slightly lower (<10 MPa) than the lithostatic pressure, similar to the results of Zierenberg *et al.* (2013). To summarize, the pressures calculated via VolatileCalc and rhyolite-MELTS yield pressures greater than the hydrostatic pressure and lower than the lithostatic pressure. In both cases, calculated pressures are closer to the lithostatic pressure (50-57 MPa) than to the hydrostatic pressure (16 MPa).

Constraints from glass compositions

When represented on a normalized anhydrous basis, the SiO_2 contents of the Krafla glass compositions have relatively low SiO_2 concentrations (i.e., 76.7 wt% SiO_2), much lower than what would be expected from the correlation between SiO_2 and pressure found by Gualda and Ghiorso (2013b), which would predict SiO_2 values >78 wt% for such low pressures. This is easily explained by the much higher FeO values (2.9 wt% FeO for the average Krafla glass; see supplementary material) observed in the tholeiitic compositions when compared to more typical calc-alkaline systems studied by Gualda and Ghiorso (2013b), which only have 0.55-1.29 wt% FeO. In this case, the SiO_2 concentration alone cannot be used for estimation of crystallization pressure using the relationship of Gualda & Ghiorso (2013b XX).

The projection scheme of Blundy and Cashman (2001) circumvents the issue of high FeO values of the Krafla compositions by employing normative values for Qz', Ab', Or', and An (effectively this means compositions are considered on an FeO-free, MgO-free basis). While the Qz'-Ab'-Or' ternary projection diagram is a somewhat crude measure of pressure, the average Krafla IDDP-1 composition lies on the 50 MPa (1.9-2.0 km) cotectic (Figure 2), which indicates that the cotectic is in good agreement with the natural samples intercepted at 2.1 km. Importantly, pressures estimated using the Qz'-Ab'-Or' ternary are maximum pressures, given that the presence of quartz is not observed in the samples.

Constraints from rhyolite-MELTS geobarometry

For the rhyolite-MELTS results, the average P_4 QFOM pressure for the individual compositions is in excellent agreement with the drilling depth. The average P_3 QFO pressure and P_3 QFM pressure for the individual compositions are also in very good agreement with the observed depth. In addition to the pressure measurements, rhyolite-MELTS estimates the f_{O2} of the Krafla system to be between ΔNNO = -0.5 and -1, which agrees with the reducing f_{O2} estimates for Krafla magmas (Nicholson, 1990; Shorttle *et al.*, 2015; Hartley *et al.*, 2017). The results from the individual and average compositions are supported by the Monte Carlo results, which yield P_4 QFOM pressures exclusively for f_{O2} of ΔNNO = -1 and -0.5. In summary, rhyolite-MELTS calculations indicate storage pressures of <55 MPa, under reducing (ΔNNO = -1 to -0.5) conditions. Furthermore, comparison of rhyolite-MELTS pressures with the fluid-saturation pressures of Zierenberg *et al.* (2013) suggests that Krafla IDDP-1 magmas were fluid-saturated, or very nearly so.

There are two notable discrepancies between the reported mineral assemblage in the Krafla IDDP-1 samples and rhyolite-MELTS calculations. First, the P_4 QFOM pressure results suggest that quartz is in equilibrium with the Krafla magmas despite no quartz being observed; as well, the pyroxene predicted by rhyolite-MELTS is orthopyroxene instead of the observed augite + pigeonite assemblage (Zierenberg *et al.*, 2013; Masotta *et al.*, 2018). While quartz has not been reported as part of the phenocryst assemblage within the mm-sized glass shards (Zierenberg *et al.*, 2013; Masotta *et al.*, 2018), the small glass shards could make it very difficult to find any phenocrystic quartz crystals. However, we do not suggest that Zierenberg *et al.* (2013 and Masotta *et al.* (2018) missed the presence of quartz. Instead, a plausible alternative is that quartz was very near saturation and/or was saturated and kinetically suppressed. The fragments of the felsite crust directly adjacent to the melt-rich, crystal-poor magma body contain quartz and alkali feldspar (and plagioclase, augite, and titano-magnetite) (Zierenberg *et al.*, 2013), suggesting that Krafla magmas were in contact with quartz-bearing rocks. This proximity to a quartz-bearing felsite could have altered the composition of the melt during storage. The coincidence of the plagioclase and quartz saturation curves for the Krafla IDDP-1 compositions indicates that both minerals are saturated in rhyolite-MELTS calculations. Importantly, the only pressures that are consistent with the rhyolite-MELTS calculations are pressures lower than the calculated pressures. As such, similarly to the case of the haplogranitic ternary, we conclude that pressures are <55 MPa.

Second, the pyroxenes observed in the Krafla IDDP-1 samples (augite + pigeonite) are both clinopyroxene. However, the rhyolite-MELTS calculations do not produce clinopyroxene for any conditions tested. Instead, the orthopyroxene saturation curve is ubiquitously present in rhyolite-MELTS calculations. For P_4 QFOM, the orthopyroxene saturation curve is coincident with the quartz + plagioclase + magnetite saturation curves. We conducted several rhyolite-MELTS runs on the average composition while suppressing orthopyroxene. In the case of f_{O2} equal to ΔNNO = -1, the four-phase intersection of quartz, plagioclase, clinopyroxene, and magnetite (P_4 QFCM) is 50 MPa, which is in excellent agreement with the P_4 QFOM pressures. Therefore, we suggest that the orthopyroxene predicted by rhyolite-MELTS is a good proxy for the low-Ca clinopyroxene present in the natural samples in Krafla magmas. Energetically, they are almost indistinguishable by rhyolite-MELTS for these Krafla compositions. It is also relevant to note that recent experimental results suggest that the clinopyroxene model in rhyolite-MELTS may be inaccurate for high-silica rhyolite compositions (Brugman and Till, 2019). Interestingly, our results suggest that – in this case – orthopyroxene is a useful proxy for clinopyroxene stability.

Very shallow magma bodies as part of transcrustal magmatic systems

There is a growing body of evidence to suggest that magmatic systems span a significant range of storage depths within the crust – leading to the idea of transcrustal magma systems (Annen *et al.*, 2006; Annen, 2009; Cashman and Giordano, 2014; Menand *et al.*, 2015; Mutch *et al.*, 2019; Svoboda *et al.*, 2021; Giordano and Caricchi, 2022). The existence of very shallow magma bodies indicates that we must extend our model of storage to a shallower level.

It is interesting to consider why these bodies have been largely underappreciated to date, with much more attention being paid to deeper levels of rhyolitic magmatic systems. The lifetimes of shallow melt-dominated magma bodies are short (Gualda *et al.*, 2012b, 2018; Cooper and Kent, 2014; Pamukçu *et al.*, 2015a, 2021; Gualda and Sutton, 2016; Pitcher *et al.*, 2021), especially when a geothermal reservoir is present (Kelly *et al.*, 2021). We speculate that very shallow magma bodies could commonly be a minor contribution to major eruptions. Their proximity to the Earth's surface makes them economically and societally important, especially from a volcanic hazards perspective.

The very shallow storage pressures calculated here are from Krafla in the plume-affected mid-ocean rift of Iceland. Shallow magmas are also inferred to exist in the rifted arc of the TVZ in Aotearoa New Zealand (Bégué *et al.*, 2014b; Gualda *et al.*, 2018; Harmon *et al.*, 2024). For both Krafla and the TVZ, the magma systems are long-lived and indicate that there is a consistent high heat flux to the shallow crust (Jonasson, 1994; Wilson, 1996; Mutch *et al.*, 2019; Kelly *et al.*, 2021), consistent with involvement of greater depths of the crust in the generation and storage of eruption-forming magma bodies (Gualda *et al.*, 2018, 2019; Smithies *et al.*, 2023).

Implications for global shallow magmatism

In addition to drilling evidence of very shallow magma at depths between 2.1 and 2.6 km at Puna, Hawaii (Teplow *et al.*, 2009), Menengai Caldera, Kenya (Mbia *et al.*, 2015), and Krafla geothermal system, Iceland (Mortensen *et al.*, 2010; Elders *et al.*, 2011; Zierenberg *et al.*, 2013), the potential presence of very shallow silicic magma has also been captured by 2D and 3D seismic exploration at the Larderello geothermal field, Italy (Cameli *et al.*, 1993; Manzella *et al.*, 2017; Rochira *et al.*, 2018) and by InSAR data at the Dabbahu volcano, Afar, Ethiopia (Ebinger *et al.*, 2008). Geophysical methods, including seismic data and InSAR, are likely critical for determining the presence of current, very shallow magma bodies.

In addition to the direct evidence at drilled magma sites, the rhyolite-MELTS evidence from previous eruptions in the TVZ, and the indirect observations by geophysical methods, there is substantial field and petrologic evidence (mostly Al-in-hornblende and Qz'-Ab'-Or' barometry, as well as common granophyric textures) for very shallow magma bodies in the plutonic record. We briefly summarize some examples below.

In the case of the Searchlight pluton in Nevada (Bachl *et al*. 1991, Wallrich *et al*. 2023), which is exposed along steeply tilted crustal sections, the upper units of the pluton intruded into roughly coeval volcanic rocks, suggesting very shallow emplacement. Further, Al-in-hornblende geobarometry suggests that the roof of the pluton was at a depth of ~3 km (Bachl *et al.*, 2001; Wallrich *et al.*, 2023). The Geysers in California is one of the world's most active geothermal fields and has a plutonic history that includes shallow intrusions ~0.2-2.8 km depth, exemplifying the connection between shallow plutonism and geothermal energy production (Angeles-De La Torre, *et al.*, 2023). In the case of the Turkey Creek and Silver Creek calderas in Arizona, resurgent monzonite and granite intruded at very shallow levels (<~2 km) (du Bray and Pallister, 1999; Ferguson *et al.*, 2013; McDowell *et al.*, 2014; Deering *et al.*, 2016). The Mount Scott Granite, Oklahoma, is interpreted to have been emplaced into comagmatic Carlton Rhyolite at a depth of no more than ~1.5 km (Hogan and Gilbert, 1995; Hogan *et al.*, 1998). The emplacement depth of Cretaceous granitoid plutons in eastern Zhejiang, China is estimated to have been at 50-100 MPa (~2-4 km) based on the Qz'-Ab'-Or' ternary (Chen *et al.*, 2021). Al-in-hornblende geobarometry yields emplacement depths of ~4-5 km at the top of the Rayo Bisco-Huemul plutonic complex, Chile (Nelson *et al.*, 1999; Schaen *et al.*, 2017). The granitic intrusions of eastern Iceland (Austurhorn, Vesturhorn, Slaufrudalur, and Reyðarártindur plutons) are all interpreted to have been emplaced into slightly older basaltic strata at depths of <~2 km, based on depths to reconstructed paleosurfaces and metamorphism (Walker, 1960, 1974; Blake, 1966; Furman *et al.*, 1992; Burchardt *et al.*, 2012; Padilla *et al.*, 2016; Twomey *et al.*, 2020; Rhodes *et al.*, 2021). Granophyric lithic blocks within pumiceous pyroclastic flows are interpreted to have formed in the magma body beneath Alid Volcanic Center, Eritrea, at a depth of 2-4 km based on geological constraints and CO_2-H_2O concentrations in melt inclusions (Lowenstern *et al.*, 1997). It is noteworthy that many of these localities are significantly affected by extension, which could suggest that extension and rifting may facilitate establishment of these very shallow magma bodies. Overall, the evidence above suggests that very shallow rhyolitic magma bodies are relatively common, and it is critical to better understand them for hazard assessment and economic exploration. As well, these very shallow magma bodies are probably important components of transcrustal magma systems that deserve further study.

Methods to petrologically and geophysically monitor the existence and the potential hazards associated with these very shallow magma bodies should be established to mitigate volcanic hazards. The substantial petrologic evidence that these magma bodies not only exist but are relatively widespread should be a call for the combined use of geophysics, hazard assessment, and petrology to properly assess the presence, properties, and potential societal impacts of very shallow magma bodies, especially as we begin to directly probe these magmas (Eichelberger *et al.*, 2018; Lavallée *et al.*, 2023). This environment has been underappreciated as a potential magma storage zone, with implications for volcanic hazards and geothermal resources.

Conclusions

In this study, we test rhyolite-MELTS geobarometry on the shallow magma intersected and retrieved from Krafla IDDP-1 geothermal well. Using the glass compositions as the input, we search for mineral-melt equilibrium conditions in temperature, pressure, and f_{O2} space to calculate the storage conditions of these magmas. Rhyolite-MELTS returns four-phase (quartz, plagioclase, orthopyroxene, magnetite; P_4 QFOM) pressures of 42 MPa (1.6-1.7 km) for ΔNNO = -0.75 and 46 MPa (1.7-1.9 km) for ΔNNO = -1, which is in excellent agreement with the drilled depth of 2.1 km. While rhyolite-MELTS calculates both quartz and orthopyroxene (instead of augite + pigeonite) to be in equilibrium with melt of the input composition, these phases are not observed in the samples. Despite these discrepancies, we argue that rhyolite-MELTS performs with high precision for this system.

The fact that we can obtain rhyolite-MELTS pressures consistent with the drilled depth lends support to rhyolite-MELTS results in other systems that produce very shallow pressures, like the Taupō Volcanic Zone, Aotearoa New Zealand. We show that rhyolite-MELTS can be used to calculate not only the pressures of storage based on a variety of mineral assemblages, but that it can also help constrain other intensive parameters such as f_{O2} and H_2O-saturation during pre-eruptive storage.

Contemporary very shallow magma bodies are confirmed in several locations, including the Krafla IDDP-1 well, and they may be relatively common features of transcrustal magmatic systems, including from the TVZ.

Coupling the magmatic information revealed by very shallow magma bodies with geophysical models and volcanic hazard assessments has broad implications for both geothermal energy production and volcanic hazards. Further, if we know the depths and conditions of these magma bodies (e.g., by using rhyolite-MELTS), we can better understand the arrangement of melt-dominated magma bodies during ongoing eruptions. This updated perspective will aid in reconfiguring conceptual models and refine the focus of eruption monitoring platforms for silicic magma storage in the upper crust.

Acknowledgments

We thank John Eichelberger for the inspiration for this project. Thanks to Mark Ghiorso for comments on an early draft and for discussion of some of the results. Thank you to the PUMMUS group for comments on early drafts and support.

Funding

There was no external funding for this project.

Author contributions

Conceptualization: BMW, GARG, LJH, CFM

Methodology: LJH, GARG, BMW

Investigation: LJH, GARG, BMW, CFM

Visualization: LJH, GARG

Supervision: GARG, LJH

Writing—original draft: LJH

Writing—review & editing: LJH, GARG, CFM, BMW

Competing interests

Authors declare that they have no competing interests.

Data and materials availability

All data are available in the main text or the supplementary materials.

References

Angeles-De La Torre, C. A., Schmitt, A. K., Lovera, O. M., Gassert, H., Gerdes, A., & Harvey, J. C. (2023). A common magma source for plutonic and volcanic rocks of the Geysers geothermal field, California: Volume and intrusive history derived from zircon. *Chemical Geology*. **624**, 121414.

Anderson, A. T. Jr., Davis, A. M., & Lu, F. (2000) Evolution of Bishop Tuff rhyolitic magma based on melt and magnetite inclusions and zoned phenocrysts. *Journal of Petrology*. **41** (3), 449-473.

Annen, C. (2009). From plutons to magma chambers: Thermal constraints on the accumulation of eruptible silicic magma in the upper crust. *Earth and Planetary Science Letters*. **284**, 409–416.

Annen, C., Blundy, J. D. & Sparks, R. S. J. (2006). The genesis of intermediate and silicic magmas in deep crustal hot zones. *Journal of Petrology*. **47**, 505–539.

Árnadóttir, T., Sigmundsson, F. & Delaney, P. T. (1998). Sources of crustal deformation associated with the Krafla, Iceland, eruption of September 1984. *Geophysical Research Letters*. **25**, 1043–1046.

Árnason, K. (2020). New Conceptual Model for the Magma-Hydrothermal-Tectonic System of Krafla, NE Iceland. *Geosciences 2020, Vol. 10, Page 34*. Multidisciplinary Digital Publishing Institute **10**, 34.

Árnason, K., Vilhjálmsson, A. M. & Björnsdóttir, T. (2008). A study of the Krafla volcano using gravity, micro earthquake and MT data. *Interim ISOR Report to Landsvirkjun*.

Aspinall, W. & Blong, R. (2015). Volcanic Risk Assessment. *The Encyclopedia of Volcanoes*. 1215–1231.

Bachl, C. A., Miller, C. F., Miller, J. S. & Faulds, J. E. (2001). Construction of a pluton: Evidence from an exposed cross section of the Searchlight pluton, Eldorado Mountains, Nevada. *Bulletin of the Geological Society of America* **113**, 1213–1228.

Bachmann, O. & Huber, C. (2016). Silicic magma reservoirs in the Earth's crust. *American Mineralogist*. **101**, 2377–2404.

Bégué, F., Deering, C. D., Gravley, D. M., Kennedy, B. M., Chambefort, I., Gualda, G. A. R. & Bachmann, O. (2014a). Extraction, storage and eruption of multiple isolated magma batches in the paired Mamaku and Ohakuri eruption, Taupo Volcanic Zone, New Zealand. *Journal of Petrology*. **55**, 1653–1684.

Bégué, F., Gualda, G. A. R., Ghiorso, M. S., Pamukçu, A. S., Kennedy, B. M., Gravley, D. M., Deering, C. D. & Chambefort, I. (2014b). Phase-equilibrium geobarometers for silicic rocks based on rhyolite-MELTS. Part 2: application to Taupo Volcanic Zone rhyolites. *Contributions to Mineralogy and Petrology* **168**, 1–16.

Blake, D. H. (1966). The net-veined complex of the Austurhorn Intrusion, southeastern Iceland. *The Journal of Geology* **74**, 891–907.

Blundy, J. D. & Cashman, K. V. (2001). Ascent-driven crystallisation of dacite magmas at Mount St Helens, 1980-1986. *Contributions to Mineralogy and Petrology* **140**, 631–650.

Blundy, J. D. & Holland, T. J. B. (1990). Calcic amphibole equilibria and a new amphibole-plagioclase geothermometer. *Contributions to Mineralogy and Petrology* **104**, 208–224.

Brugman, K. K. & Till, C. B. (2019) A low-aluminum clinopyroxene-liquid geothermometer for high-silica magmatic systems. *American Mineralogist* **104** (7), 996-1004.

Burchardt, S., Tanner, D. & Krumbholz, M. (2012). The Slaufrudalur pluton, southeast Iceland-An example of shallow magma emplacement by coupled cauldron subsidence and magmatic stoping. *Bulletin of the Geological Society of America* **124**, 213–227.

Calderone, G. M., Gr6nvold, K. & Oskarsson, N. (1990). The welded air-fall tuff layer at Krafla, northern Iceland: a composite eruption triggered by injection of basaltic magma. *Journal of Volcanology and Geothermal Research* **44**, 303–314.

Cameli, G. M., Dini, I. & Liotta, D. (1993). Upper crustal structure of the Larderello geothermal field as a feature of post-collisional extensional tectonics (Southern Tuscany, Italy). *Tectonophysics*. **224**, 413.

Caricchi, L., Townsend, M., Rivalta, E. & Namiki, A. (2021). The build-up and triggers of volcanic eruptions. *Nature Reviews Earth & Environment* **2**, 458–476.

Cashman, K. V & Giordano, G. (2014). Calderas and magma reservoirs. *Journal of Volcanology and Geothermal Research*. **288**, 28–45.

Cashman, K. V., Stephen, R., Sparks, J. & Blundy, J. D. (2017). Vertically extensive and unstable magmatic systems: A unified view of igneous processes. *Science* **355**.

Cassidy, M., Manga, M., Cashman, K. & Bachmann, O. (2018). Controls on explosive-effusive volcanic eruption styles. *Nature Communications*. **9**.

Cassidy, M. & Mani, L. (2022). Huge volcanic eruptions: time to prepare. *Nature*. 469–471.

Chen, J. Y., Yang, J. H., Zhang, J. H. & Zhu, Y. S. (2021). Construction of a highly silicic upper crust in southeastern China: Insights from the Cretaceous intermediate-to-felsic rocks in eastern Zhejiang. *Lithos*. **402–403**.

Cooper, K. M. & Kent, A. J. R. (2014). Rapid remobilization of magmatic crystals kept in cold storage. *Nature*. **506**, 480–483.

Deering, C. D., Keller, B., Schoene, B., Bachmann, O., Beane, R. & Ovtcharova, M. (2016). Zircon record of the plutonic-volcanic connection and protracted rhyolite melt evolution. *Geology*. **44**, 267–270.

du Bray, E. A. & Pallister, J. S. (1999). Recrystallization and anatexis along the plutonic-volcanic contact of the Turkey Creek caldera, Arizona. *GSA Bulletin* **111**, 143–153.

Ebinger, C. J., Keir, D., Ayele, A., Calais, E., Wright, T. J., Belachew, M., Hammond, J. O. S., Campbell, E. & Buck, W. R. (2008). Capturing magma intrusion and faulting processes during continental rupture: Seismicity of the Dabbahu (Afar) rift. *Geophysical Journal International*. **174**, 1138–1152.

Eichelberger, J., Ingolfsson, H., Carrigan, C., Lavallee, Y., Tester, J. & Markusson, S. (2018). Krafla magma testbed: Understanding and using the magma-hydrothermal connection. Geothermal Resources Council.

Einarsson, P. (1978). S-wave shadows in the Krafla caldera in NE-Iceland, evidence for a magma chamber in the crust. *Bulletin of Volcanology* **41**, 1–9.

Elders, W. A. *et al.* (2011). Origin of a rhyolite that intruded a geothermal well while drilling at the Krafla volcano, Iceland. *Geology* **39**, 231–234.

Ferguson, C. A., McIntosh, W. C. & Miller, C. F. (2013). Silver Creek caldera-The tectonically dismembered source of the Peach Spring Tuff. *Geology* **41**, 3–6.

Foley, M. L., Miller, C. F. & Gualda, G. A. R. (2020). Architecture of a Super-sized Magma Chamber and Remobilization of its Basal Cumulate (Peach Spring Tuff, USA). *Journal of Petrology* **61**.

Frioleifsson, G. O., Ármannsson, H., Guomundsson, Á., Árnason, K., Mortensen, A. K., Pálsson, B. & Einarsson, G. M. (2014). Site selection for the well IDDP-1 at Krafla. *Geothermics* **49**, 9–15.

Furman, T., Meyer, P. S. & Frey, F. (1992). Evolution of Icelandic central volcanoes: evidence from the Austurhorn intrusion, southeastern Iceland. *Bulletin of Volcanology* **55**, 45–62.

Ghiorso, M. S. & Gualda, G. A. R. (2015). An H_2O–CO_2 mixed fluid saturation model compatible with rhyolite-MELTS. *Contributions to Mineralogy and Petrology* **169**, 53.

Giordano, G. & Caricchi, L. (2022). Determining the State of Activity of Transcrustal Magmatic Systems and Their Volcanoes. *Annual Review of Earth and Planetary Sciences* **50**, 231–259.

Gualda, G. A. R. & Ghiorso, M. S. (2013a). The Bishop Tuff giant magma body: an alternative to the Standard Model. *Contributions to Mineralogy and Petrology* **166**, 755–775.

Gualda, G. A. R. & Ghiorso, M. S. (2013b). Low-Pressure Origin of High-Silica Rhyolites and Granites. *The Journal of Geology* **121**, 537–545.

Gualda, G. A. R. & Ghiorso, M. S. (2014). Phase-equilibrium geobarometers for silicic rocks based on rhyolite-MELTS. Part 1: Principles, procedures, and evaluation of the method. *Contributions to Mineralogy and Petrology* **168**, 1–17.

Gualda, G. A. R. & Ghiorso, M. S. (2015). MELTS-Excel: A Microsoft Excel-based MELTS interface for research and teaching of magma properties and evolution. *Geochemistry, Geophysics, Geosystems* **16**, 315–324.

Gualda, G. A. R., Ghiorso, M. S., Lemons, R. V. & Carley, T. L. (2012a). Rhyolite-MELTS: a Modified Calibration of MELTS Optimized for Silica-rich, Fluid-bearing Magmatic Systems. *Journal of Petrology* **53**, 875–890.

Gualda, G. A. R., Gravley, D. M., Conner, M., Hollmann, B., Pamukçu, A. S., Bégué, F., Ghiorso, M. S. & Deering, C. D. (2018). Climbing the crustal ladder: Magma storage-depth evolution during a volcanic flare-up. *Science Advances* **4**, eaap7567.

Gualda, G. A. R., Gravley, D. M., Deering, C. D. & Ghiorso, M. S. (2019). Magma extraction pressures and the architecture of volcanic plumbing systems. *Earth and Planetary Science Letters*. **522**, 118–124.

Gualda, G. A. R., Pamukçu, A. S., Ghiorso, M. S., Anderson Jr, A. T., Sutton, S. R. & Rivers, M. L. (2012b). Timescales of Quartz Crystallization and the Longevity of the Bishop Giant Magma Body. *PLoS ONE* **7**, e37492.

Gualda, G. A. R. & Sutton, S. R. (2016). The year leading to a supereruption. *PLoS ONE* **11**, 1–18.

Halldórsson, S. A. *et al.* (2018). Petrology and geochemistry of the 2014-2015 Holuhraun eruption, central Iceland: compositional and mineralogical characteristics, temporal variability and magma storage. **173**, 64.

Harmon, L. J., Cowlyn, J., Gualda, G. A. R. & Ghiorso, M. S. (2018). Phase-equilibrium geobarometers for silicic rocks based on rhyolite-MELTS. Part 4: Plagioclase, orthopyroxene, clinopyroxene, glass geobarometer, and application to Mt. Ruapehu, New Zealand. *Contributions to Mineralogy and Petrology* **173**, 7.

Harmon, L. J., Gualda, G. A. R., Gravley, D. M., Smithies, S. L. & Deering, C. D. (2024). The Whakamaru magmatic system (Taupō Volcanic Zone, New Zealand), part 1: Evidence from tephra deposits for the eruption of multiple magma types through time. *Journal of Volcanology and Geothermal Research*. **445**, 107966.

Hartley, M. E., Shorttle, O., Maclennan, J., Moussallam, Y. & Edmonds, M. (2017). Olivine-hosted melt inclusions as an archive of redox heterogeneity in magmatic systems. *Earth and Planetary Science Letters*. **479**, 192–205.

Hogan, J. P. & Gilbert, M. C. (1995). The A-type Mount Scott granite sheet: importance of crustal magma traps. *Journal of Geophysical Research* **100**.

Hogan, J. P., Price, J. D. & Gilbert, M. C. (1998). Magma traps and driving pressure: consequences for pluton shape and emplacement in an extensional regime. *Journal of Structural Geology* **20**, 1155–1168.

Hollingsworth, J., Leprince, S., Ayoub, F. & Avouac, J. P. (2012). Deformation during the 1975-1984 Krafla rifting crisis, NE Iceland, measured from historical optical imagery. *Journal of Geophysical Research: Solid Earth* **117**.

Huber, C., Townsend, M., Degruyter, W. & Bachmann, O. (2019). Optimal depth of subvolcanic magma chamber growth controlled by volatiles and crust rheology. *Nature Geoscience*. **12**, 762–768.

Jonasson, K. (1994). Rhyolite volcanism in the Krafla central volcano, north-east Iceland. *Bulletin of Volcanology*. **56**, 516–528.

Jorgenson, C., Higgins, O., Petrelli, M., Bégué, F. & Caricchi, L. (2022). A Machine Learning-Based Approach to Clinopyroxene Thermobarometry: Model Optimization and Distribution for Use in Earth Sciences. *Journal of Geophysical Research: Solid Earth*. **127**.

Kelly, L. J., Gualda, G. A. R., Gravley, D. M. & Dempsey, D. E. (2021). Hydrothermal Cooling as a Requirement for Short Storage of Silicic Magmas. *Geochemistry, Geophysics, Geosystems*. **22**.

Kennedy, B. M., Holohan, E. P., Stix, J., Gravley, D. M., Davidson, J. R. J. & Cole, J. W. (2018). Magma plumbing beneath collapse caldera volcanic systems. *Earth-Science Reviews*. 404–424.

Lavallée, Y. *et al.* (2023). Implementing the Krafla Magma Testbed (KMT): linking volcanology and geothermal research for future hazard and energy solutions. *EGU23*. Copernicus Meetings.

Lees, J. M. (2007). Seismic tomography of magmatic systems. *Journal of Volcanology and Geothermal Research* **167**, 37–56.

Lerner, A. H., O'Hara, D., Karlstrom, L., Ebmeier, S. K., Anderson, K. R. & Hurwitz, S. (2020). The Prevalence and Significance of Offset Magma Reservoirs at Arc Volcanoes. *Geophysical Research Letters*. **47**.

Lowenstern, J. B., Clynne, M. A. & Bullen, T. D. (1997). Comagmatic A-type granophyre and rhyolite from the Alid Volcanic Center, Eritrea, northeast Africa. *Journal of Petrology* **38**, 1707–1721.

Lowenstern, J. B., Smith, R. B. & Hill, D. P. (2006). Monitoring super-volcanoes: geophysical and geochemical signals at Yellowstone and other large caldera systems. *Philosophical Transactions of the Royal Society* **364**, 2055–2072.

Manzella, A. *et al.* (2017). Data integration and conceptual modelling of the Larderello geothermal area, Italy. *EGU General Assembly Conference Abstracts*, 19034.

Masotta, M., Mollo, S., Nazzari, M., Tecchiato, V., Scarlato, P., Papale, P. & Bachmann, O. (2018). Crystallization and partial melting of rhyolite and felsite rocks at Krafla volcano: A comparative approach based on mineral and glass chemistry of natural and experimental products. *Chemical Geology*. **483**, 603–618.

Mbia, P. K., Mortensen, A. K., Oskarsson, N., Bjorn, S. & Hardarson, B. S. (2015). Sub-Surface Geology, Petrology and Hydrothermal Alteration of the Menengai Geothermal Field, Kenya: Case Study of Wells MW-02, MW-04, MW-06 and MW-07. *Proceedings World Geothermal Congress*. Melbourne, Australia.

McDowell, S. M., Miller, C. F., Mundil, R., Ferguson, C. A. & Wooden, J. L. (2014). Zircon evidence for a ~200 k.y. supereruption-related thermal flare-up in the Miocene southern Black Mountains, western Arizona, USA. *Contributions to Mineralogy and Petrology*. **168**, 1–21.

Menand, T., Annen, C. & Blanquat, M. de Saint (2015). Rates of magma transfer in the crust: Insights into magma reservoir recharge and pluton growth. *Geology* **43**, 199–202.

Miller, C. F. & Wark, D. A. (2008). Supervolcanoes and their explosive supereruptions. *Elements* **4**, 11–16.

Moore, G. (2008). Interpreting H2O and CO2 Contents in Melt Inclusions: Constraints from Solubility Experiments and Modeling. *Reviews in Mineralogy and Geochemistry* **69**, 333–362.

Mortensen, A. K., Grönvold, K., Gudmundsson, Á., Steingrímsson, B. & Egilson, T. (2010). Quenched Silicic Glass from Well KJ-39 in Krafla, North-Eastern Iceland. *Proceedings World Geothermal Congress*.

Mutch, E.J.F., Blundy, J.D., Tattitch, B.C., Cooper F.J., Brooker, R.A. (2016) An experimental study of amphibole stability in low-pressure granitic magmas and a revised Al-in-hornblende geobarometer. *Contributions to Mineralogy and Petrology.* **171**, 85.

Mutch, E. J. F., Maclennan, J., Shorttle, O., Edmonds, M. & Rudge, J. F. (2019). Rapid transcrustal magma movement under Iceland. *Nature Geoscience*. **12**, 569–574.

Neave, D. A. & Putirka, K. D. (2017). A new clinopyroxene-liquid barometer, and implications for magma storage pressures under Icelandic rift zones. *American Mineralogist*. **102**, 777–794.

Nelson, S. T., Davidson, J. P., Heizler, M. T. & Kowallis, B. J. (1999). Tertiary tectonic history of the southern Andes: The subvolcanic sequence to the Tatara-San Pedro volcanic complex, lat 36S. *GSA Bulletin* **111**, 1387–1404.

Newman, S. & Lowenstern, J. B. (2002). VOLATILECALC: A silicate melt-H2O-CO2 solution model written in Visual Basic for excel. *Computers and Geosciences* **28**, 597–604.

Nicholson, H. (1990). The magmatic evolution of Krafla, NE Iceland. Edinburgh, University of Edinburgh.

Nimis, P. & Ulmer, P. (1998). Clinopyroxene geobarometry of magmatic rocks Part 1: An expanded structural geobarometer for anhydrous and hydrous, basic and ultrabasic systems. *Contributions to Mineralogy and Petrology* **133**, 122–135.

Padilla, A.J., Miller, C.F., Carley, T.L., Economos, R.C., Schmitt, A. K., Coble, M. A., Wooden, J. L., Fisher, C. M., Vervoort, J. D., Hanchar, J. M. (2016) Elucidating the magmatic history of the Austurhorn silicic intrusive complex (southeast Iceland) using zircon elemental and isotopic geochemistry and geochronology. *Contributions to Mineralogy and Petrology* **171**, 69.

Pamukçu, A. S., Gualda, G. A. R., Bégué, F. & Gravley, D. M. (2015a). Melt inclusion shapes: Timekeepers of short-lived giant magma bodies. *Geology* **43**, 947–950.

Pamukçu, A. S., Gualda, G. A. R., Ghiorso, M. S., Miller, C. F. & McCracken, R. G. (2015b). Phase-equilibrium geobarometers for silicic rocks based on rhyolite-MELTS—Part 3: Application to the Peach Spring Tuff (Arizona–California–Nevada, USA). *Contributions to Mineralogy and Petrology* **169**, 1–17.

Pamukçu, A. S., Gualda, G. A. R. & Gravley, D. M. (2021). Rhyolite-MELTS and the storage and extraction of large-volume crystal-poor rhyolitic melts at the Taupō Volcanic Center: a reply to Wilson et al. (2021). *Contributions to Mineralogy and Petrology*. **176**.

Pamukçu, A. S., Wright, K. A., Gualda, G. A. R. & Gravley, D. (2020). Magma residence and eruption at the Taupo Volcanic Center (Taupo Volcanic Zone, New Zealand): insights from rhyolite-MELTS geobarometry, diffusion chronometry, and crystal textures. *Contributions to Mineralogy and Petrology*. **175**.

Paulatto, M., Hooft, E. E. E., Chrapkiewicz, K., Heath, B., Toomey, D. R. & Morgan, J. V. (2022). Advances in seismic imaging of magma and crystal mush. *Frontiers in Earth Science* **10**, 970131.

Petrelli, M., Caricchi, L. & Perugini, D. (2020). Machine Learning Thermo-Barometry: Application to Clinopyroxene-Bearing Magmas. *Journal of Geophysical Research: Solid Earth*. **125**.

Pitcher, B. W., Gualda, G. A. R. & Hasegawa, T. (2021). Repetitive Duality of Rhyolite Compositions, Timescales, and Storage and Extraction Conditions for Pleistocene Caldera-forming Eruptions, Hokkaido, Japan. *Journal of Petrology*. Oxford University Press **62**, egaa106.

Polacci, M. *et al.* (2017). From magma ascent to ash generation: investigating volcanic conduit processes by integrating experiments, numerical modeling, and observations. *Annals of Geophysics*, **60**, 6.

Putirka, K. (2016a). Special collection: Rates and depths of magma ascent on earth: Amphibole thermometers and barometers for igneous systems and some implications for eruption mechanisms of felsic magmas at arc volcanoes. *American Mineralogist*. Walter de Gruyter GmbH **101**, 841–858.

Putirka, K. (2016b). Amphibole thermometers and barometers for igneous systems and some implications for eruption mechanisms of felsic magmas at arc volcanoes. *American Mineralogist* **101**, 841–858.

Putirka, K. D. (2008). Thermometers and Barometers for Volcanic Systems. *Reviews in Mineralogy and Geochemistry* **69**, 61–120.

Putirka, K. D., Mikaelian, H., Ryerson, F. & Shaw, H. (2003). New clinopyroxene-liquid thermobarometers for mafic, evolved, and volatile-bearing lava compositions, with applications to lavas from Tiber and the Snake River Plain, Idaho. *American Mineralogist* **88**, 1542–1554.

Rhodes, E. L. *et al.* (2021). Rapid Assembly and Eruption of a Shallow Silicic Magma Reservoir, Reyðarártindur Pluton, Southeast Iceland. *Geochemistry, Geophysics, Geosystems* **22**.

Rochira, F., Caggianelli, A. & de Lorenzo, S. (2018). Regional thermo-rheological field related to granite emplacement in the upper crust: implications for the Larderello area (Tuscany, Italy). *Geodinamica Acta* **30**, 225–240.

Rooyakkers, S. M., Stix, J., Berlo, K. & Barker, S. J. (2019). Emplacement of unusual rhyolitic to basaltic ignimbrites during collapse of a basalt-dominated caldera: The Halarauður eruption, Krafla (Iceland). *Bulletin* **132**(9-10), 1881-1902.

Rooyakkers, S. M., Stix, J., Berlo, K., Petrelli, M., Hampton, R. L., Barker, S. J. & Morgavi, D. (2021). The Origin of Rhyolitic Magmas at Krafla Central Volcano (Iceland). *Journal of Petrology*. **62**.

Sæmundsson, K. (1991). The Natural History of Lake Myvatn. *Geology of the Krafla system*, 24–95.

Sæmundsson, K. & Pringle, M. S. (2000). Um aldur berglaga Í Kröflukerfinu (On the age of rock strata in the Krafla system). *Proceedings of the Geoscience Society of Iceland Spring Meeting Abstracts*. Reykjavík, 26–27.

Saubin, E. *et al.* (2021). Textural and geochemical window into the IDDP-1 rhyolitic melt, Krafla, Iceland, and its reaction to drilling. *Bulletin of the Geological Society of America*. **133**, 1815–1830.

Schaen, A. J., Cottle, J. M., Singer, B. S., Brenhin Keller, C., Garibaldi, N. & Schoene, B. (2017). Complementary crystal accumulation and rhyolite melt segregation in a late Miocene Andean pluton. *Geology*. **45**, 835–838.

Schmidt, M. W. (1992). Amphibole composition in tonalite as a function of pressure: An experimental calibration of the Al-in-hornblende barometer. *Contributions to Mineralogy and Petrology* **110**, 304–310.

Self, S. (2006). The effects and consequences of very large explosive volcanic eruptions. *Philosophical Transactions of the Royal Society A: Mathematical, Physical and Engineering Sciences* **364**, 2073–2097.

Seropian, G., Schipper, C. I., Harmon, L. J., Smithies, S. L., Kennedy, B. M., Castro, J. M., Alloway, B. V. & Forte, P. (2021). A century of ongoing silicic volcanism at Cordón Caulle, Chile: New constraints on the magmatic system involved in the 1921–1922, 1960 and 2011–2012 eruptions. *Journal of Volcanology and Geothermal Research*. **420**.

Shorttle, O., Moussallam, Y., Hartley, M. E., Maclennan, J., Edmonds, M. & Murton, B. J. (2015). Fe-XANES analyses of Reykjanes Ridge basalts: Implications for oceanic crust's role in the solid Earth oxygen cycle. *Earth and Planetary Science Letters*. **427**, 272–285.

Smithies, S. L., Harmon, L. J., Allen, S. M., Gravley, D. M. & Gualda, G. A. R. (2023). Following magma: The pathway of silicic magmas from extraction to storage during an ignimbrite flare-up, Taupō Volcanic Zone, New Zealand. *Earth and Planetary Science Letters*. **607**, 118053.

Svoboda, C., Rooney, T. O., Girard, G. & Deering, C. (2021). Transcrustal magmatic systems: evidence from andesites of the southern Taupo Volcanic Zone. *Journal of the Geological Society*. **179**, jgs2020-204.

Teplow, W., Marsh, B., Hulen, J., Spielman, P., Kaleikini, M., Fitch, D. & Rickard, W. (2009). Dacite melt at the Puna Geothermal Venture wellfield, Big Island of Hawaii. *GRC Transactions* **33**.

Thomas, W. M. & Ernst, W. G. (1990). The aluminum content of hornblende in calc-alkaline granitic rocks: A mineralogic barometer calibrated experimentally to 12 kbars. *Geochemical Society Special Publication* **Fluid-Mine**, 59–63.

Thorarinsson, S. (1979). The Postglacial History of the Mývatn Area. *Oikos*. **32**, 16.

Till, C. B., Vazquez, J. A. & Boyce, J. W. (2015). Months between rejuvenation and volcanic eruption at Yellowstone caldera, Wyoming. *Geology*. **43**, 695–698.

Tilling, R. I. (2008). The critical role of volcano monitoring in risk reduction. *Advances in Geosciences*, **14**, 3-11.

Townsend, M. & Huber, C. (2020). A critical magma chamber size for volcanic eruptions. *Geology* **48**, 431–435.

Tramontano, S., Gualda, G. A. R. & Ghiorso, M. S. (2017). Internal triggering of volcanic eruptions: tracking overpressure regimes for giant magma bodies. *Earth and Planetary Science Letters* **472**, 142–151.

Twomey, V., McCarthy, W., Magee, C. & Petronis, M. (2020). Pre-existing fault-controlled eruptions from the lateral tips of a laccolith in SE Iceland. *Copernicus Meetings*.

Walker, G. P. L. (1960). Zeolite Zones and Dike Distribution in Relation to the Structure of the Basalts of Eastern Iceland. *The Journal of Geology* **68**, 515–528.

Walker, G. P. L. (1974). The Structure of Eastern Iceland. In: Kristjansson, L. (ed.) *Geodynamics of Iceland and the North Atlantic Area*. 177–188.

Wallace, P. J., Anderson, A. T. Jr., Davis, A. M. (1999). Gradients in H_2O, CO2, and exsolved gas in a large-volume silicic magma system: interpreting the record preserved in melt inclusions in the Bishop Tuff. *Journal of Geophysical Research: Solid Earth* **104** (B9) 20097-20122.

Wallrich, B. M., Miller, C. F., Gualda, G. A. R., Miller, J. S., Hinz, N. H. & Faulds, J. E. (2023). Volcano-pluton connection: Perspectives on material and process linkages, Searchlight pluton and Highland Range volcanic sequence, Nevada, USA. *Earth-Science Reviews*. **238**, 104361.

Wieser, P. E., Kent, A. J. R., Till, C. B., Donovan, J., Neave, D. A., Blatter, D. L. & Krawczynski, M. J. (2023). Barometers Behaving Badly I: Assessing the Influence of Analytical and Experimental Uncertainty on Clinopyroxene Thermobarometry Calculations at Crustal Conditions. *Journal of Petrology*. **64**.

Wieser, P. E., Petrelli, M., Lubbers, J., Wieser, E., Özaydın, S., Kent, A. J. R. & Till, C. B. (2022). Thermobar: An open-source Python3 tool for thermobarometry and hygrometry. *Volcanica*. **5**, 349–384.

Wilson, C. J. N. (1996). Taupo's atypical arc. *Nature* **379**, 27–28.

Wright, T. J., Ebinger, C., Biggs, J., Ayele, A., Yirgu, G., Keir, D. & Stork, A. (2006). Magma-maintained rift segmentation at continental rupture in the 2005 Afar dyking episode. *Nature*. **442**, 291–294.

Zierenberg, R. A. *et al.* (2013). Composition and origin of rhyolite melt intersected by drilling in the Krafla geothermal field, Iceland. *Contributions to Mineralogy and Petrology*. **165**, 327–347.

Figure Captions and Tables

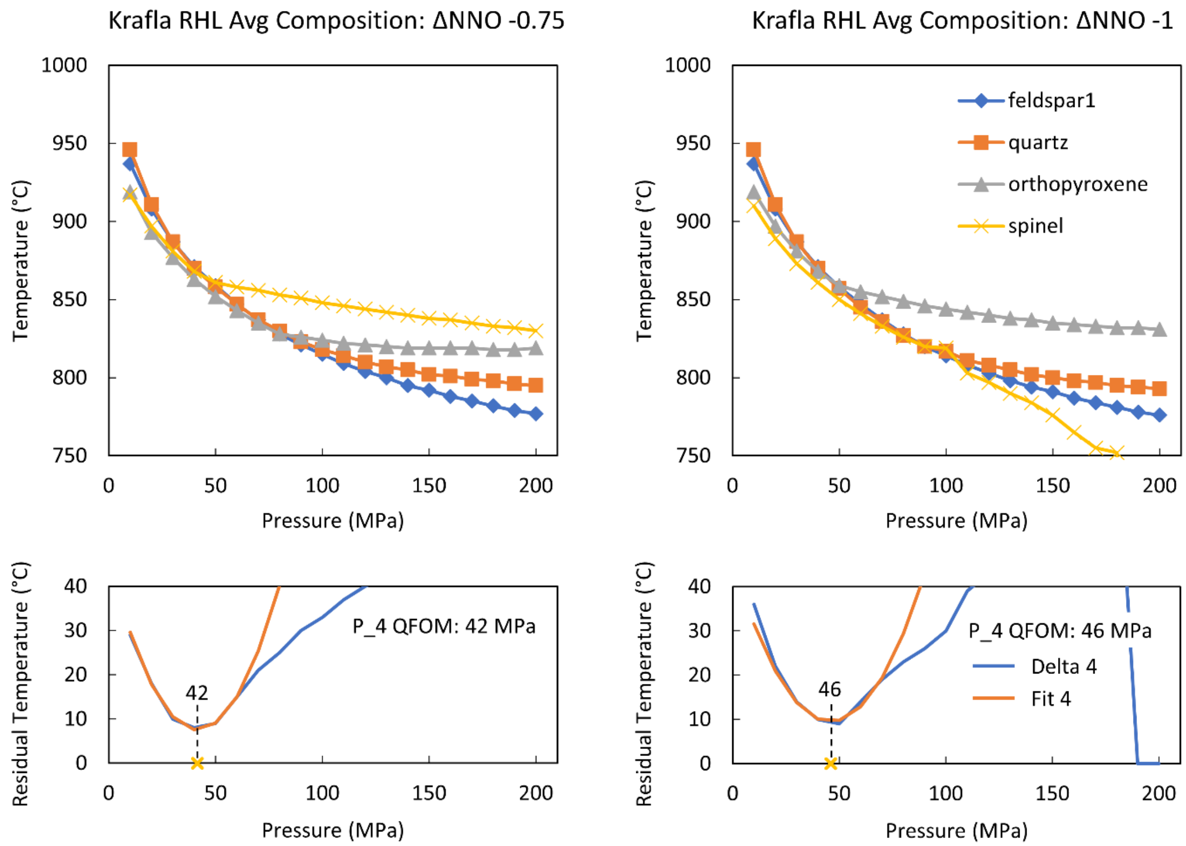

Fig. 1. Rhyolite-MELTS storage pressures for the Krafla RHL average composition as a function of oxygen fugacity. Storage pressures indicate the pressure and temperature estimates for which quartz, plagioclase, orthopyroxene, and spinel (magnetite) are simultaneously saturated (P_4 QFOM). The oxygen fugacity (f_{O2}) estimates of ΔNNO = -0.75 (left panel) and ΔNNO = -1 (right panel) are the only f_{O2} values that yield pressures for the Krafla RHL average composition, as these are the only simulations in which all four mineral phases saturate within 10 °C of each other (the residual temperature cutoff we use for a 4-phase solution, shown by the blue "Delta 4" in the lower diagrams). The pressure is calculated by fitting a parabola ("Fit 4") to the residual temperature points around the minimum residual temperature ("Delta 4"); see Gualda and Ghiorso (2014) for details. The stability of both orthopyroxene and spinel (magnetite) depends on f_{O2} due to the presence of Fe. The estimated pressures are 42 MPa and 46 MPa, respectively. Using a density of 2,500 kg/m^3, these pressures are calculated to be 1.6 km and 1.7 km; using a density of 2,700 kg/m^3, these pressures are calculated to be 1.7 km and 1.9 km.

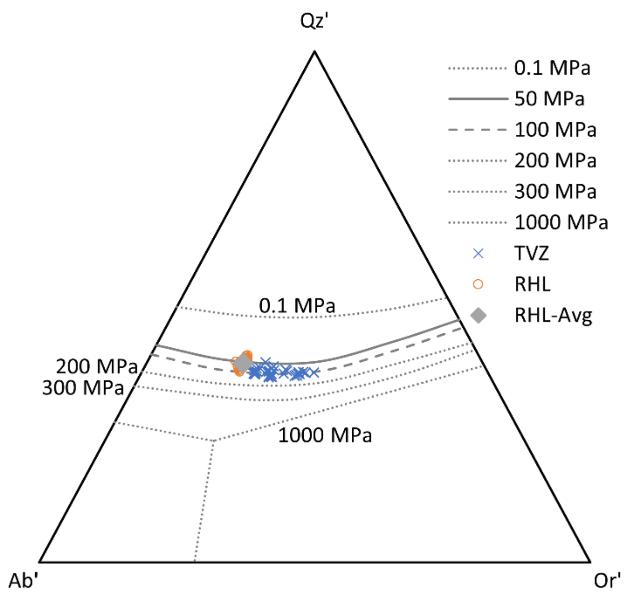

Fig. 2. Projection of glass compositions onto the quartz-albite-orthoclase (Qz'-Ab'-Or') ternary diagram. Projection of individual glass compositions and the average glass composition from Krafla RHL glass shards (Masotta *et al.*, 2018) and glass compositions from TVZ ignimbrite pumice (Bégué *et al.*, 2014; Gualda *et al.*, 2018) onto the quartz-albite-orthoclase (Qz'-Ab'-Or') ternary diagram using the projection scheme of Blundy and Cashman (2001), which relies only on the glass compositions. The Krafla RHL compositions plot mostly between the 50 MPa and 100 MPa cotectic, with the average composition plotting at ~ 50 MPa. The TVZ compositions plot mostly between 50 and ~150 MPa, predominantly around the 100 MPa cotectic. Note that the Krafla RHL compositions plot slightly shallower than TVZ compositions. Importantly, inferred pressures are maximum pressures if quartz is not in equilibrium with the melt.

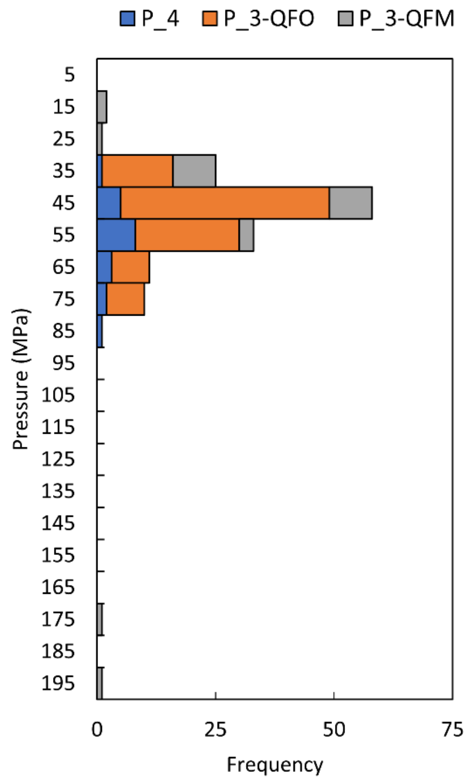

Fig. 3. Results from rhyolite-MELTS pressure modeling for all individual Krafla RHL compositions (Masotta *et al.*, 2018)**.** We report the P_4 QFOM, P_3 QFO, and P_3 QFM pressures for all f_{O2} considered. Note the narrow range of pressures that return a P_4 QFOM pressure, which is the most sensitive to f_{O2}. There is a strong mode at ~45-55 MPa for all assemblages, with slightly higher values for P_4 QFOM pressures.

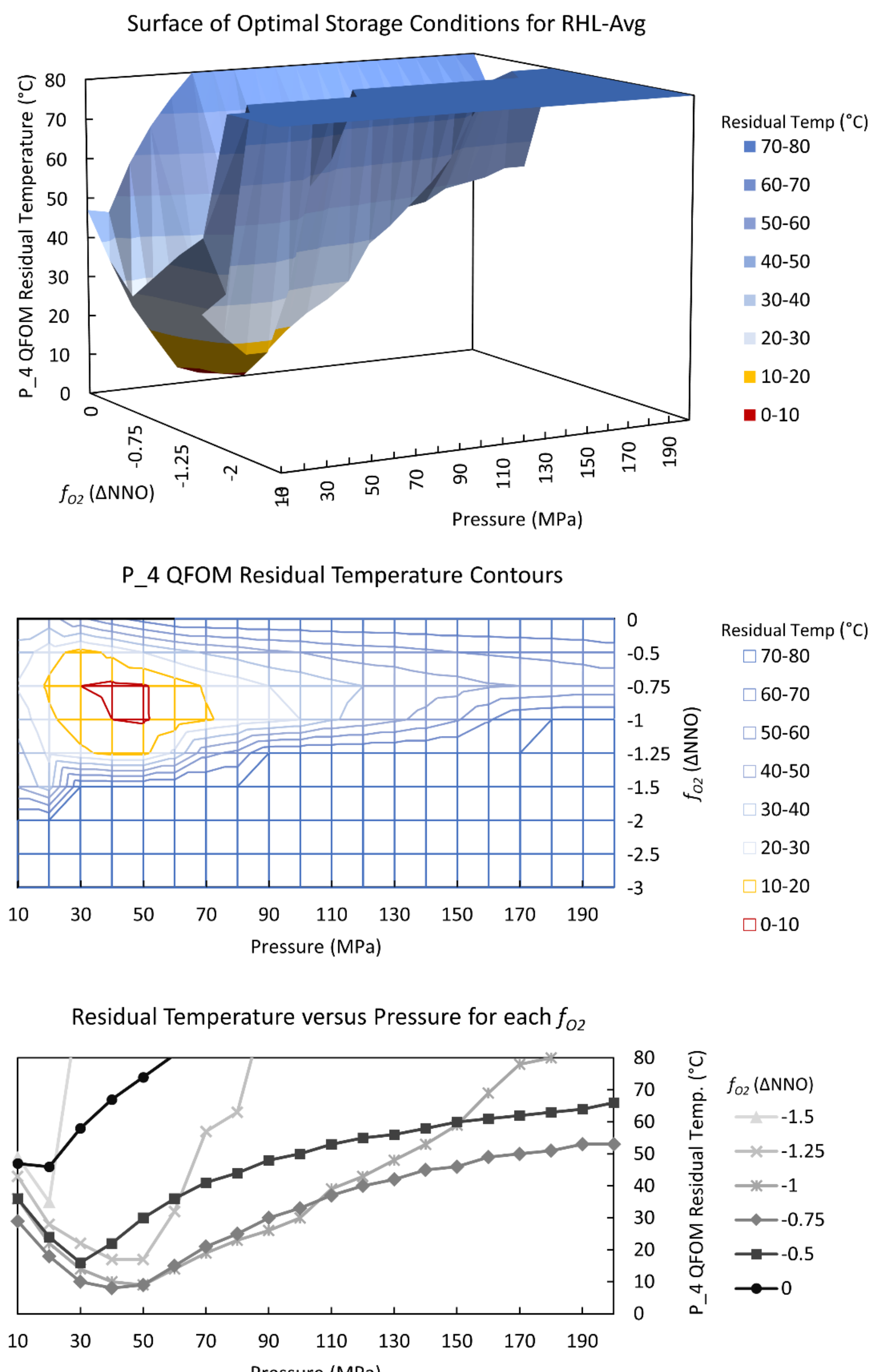

Figure 4

Fig. 4. Rhyolite-MELTS storage pressures for the Krafla RHL average glass composition, showing the effect of f_{O2} on pressure calculations. In the top panel, the central red divot (~40 MPa and ΔNNO = ~-0.75) shows the conditions that retrieves the best pressure and f_{O2} estimate

based on the lowest residual temperature when all four phases are considered (P_4 QFOM). The middle panel shows the same data as a 2D contour plot. For readability, residual values > 80 °C are shown as 80 °C. The bottom panel shows the residual temperatures (the difference between the saturation curves of different phases) for individual rhyolite-MELTS calculations, which is compiled to create the two upper panels. For most f_{O2} values, particularly between ΔNNO = -1.25 to -0.75, estimated pressures are between 40 and 50 MPa. Calculations outside this f_{O2} interval (ΔNNO < -1.5 and ΔNNO > -0.75) yield no pressures.

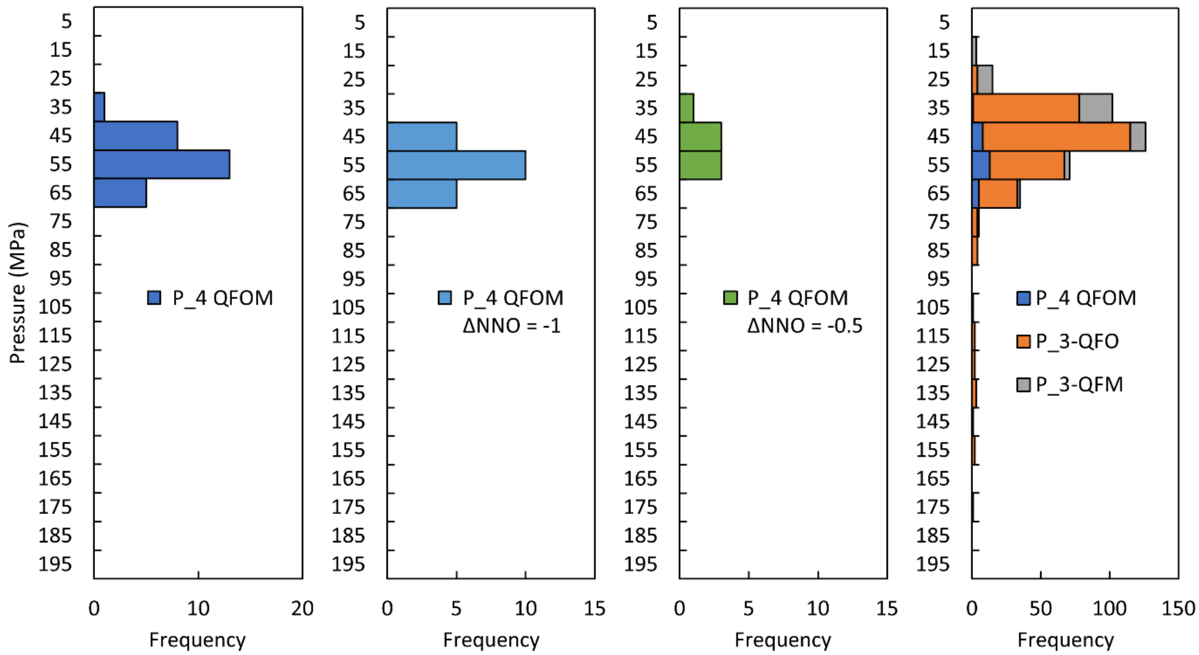

Fig. 5. Rhyolite-MELTS results for the Monte Carlo analysis. The Monte Carlo analysis included 600 synthetic compositions that varied about the mean of the Krafla RHL composition, using the calculated standard deviation, with f_{O2} values from ΔNNO = -2 to 0 distributed uniformly in 0.5 f_{O2} steps. Left panel shows rhyolite-MELTS P_4 QFOM pressure results from the Monte Carlo analysis. The only f_{O2} values that resulted in a P_4 QFOM pressure calculation are f_{O2} equal to ΔNNO -1 and ΔNNO -0.5, shown in the middle two panels. This indicates we can determine the pressure and the f_{O2} of the system. The right panel shows rhyolite-MELTS P_4 QFOM, P_3 QOF and P_3 QFM pressure results from the Monte Carlo simulations for all f_{O2} values considered. In all cases, modes of the distributions are in the 45-55 MPa bins.

(A) Mean pressure calculation (MPa) and depth (km)[1]

	-3 ΔNNO	**-2.5 ΔNNO**	**-2 ΔNNO**	**-1.5 ΔNNO**	**-1.25 ΔNNO**	**-1 ΔNNO**	**-0.75 ΔNNO**	**-0.5 ΔNNO**	**0 ΔNNO**
P_4 QFOM	-	-	-	-	-	57 MPa (2.1; 2.3 km)	47 MPa (1.8; 1.9 km)	35 MPa (1.3; 1.4 km)	-
P_3 QFO	40 MPa (1.5; 1.6 km)	42 MPa (1.6; 1.7 km)	45 MPa (1.7; 1.8 km)	47 MPa (1.8; 1.9 km)	48 MPa (1.8; 2.0 km)	49 MPa (1.9; 2.0 km)	46 MPa (1.7; 1.9 km)	35 MPa (1.3; 1.4 km)	-
P_3 QFM	-	-	-	-	-	55 MPa (2.1; 2.2 km)	60 MPa (2.3; 2.5 km)	32 MPa (1.2; 1.3 km)	9 MPa (0.4; 0.4 km)

(B) Standard deviation pressure calculation (MPa) and depth (km)[2]

P_4 QFOM	-	-	-	-	-	11 MPa (0.4; 0.5 km)	5 MPa (0.2 km)	2 MPa (0.1 km)	-
P_3 QFO	9 MPa (0.3; 0.4 km)	9 MPa (0.4; 0.4 km)	11 MPa (0.4; 0.5 km)	11 MPa (0.4; 0.5 km)	12 MPa (0.5; 0.5 km)	11 MPa (0.4; 0.5 km)	5 MPa (0.2 km)	2 MPa (0.1 km)	-
P_3 QFM	-	-	-	-	-	11 MPa (0.4; 0.5 km)	47 MPa (1.8; 1.9 km)	5 MPa (0.2 km)	1 MPa (0 km)

(C) Number of compositions that return pressures for each f_{O_2}[3]

P_4 QFOM	0	0	0	0	0	9	9	2	0
P_3 QFO	14	16	17	20	20	9	1	0	0
P_3 QFM	0	0	0	0	0	2	8	14	2

Table 1. Pressure calculations for Krafla RHL individual compositions.

[1]Mean of P_4 QFOM, P_3 QFO, and P_3 QFM storage pressures for Krafla RHL individual composition for different f_{O2} reported in MPa and km; the densities used to convert pressure to depth are 2,700 kg/m^3 and 2,500 kg/m^3

[2]Standard deviation of P_4 QFOM, P_3 QFO, and P_3 QFM storage pressures for Krafla RHL individual compositions reported in MPa and km

[3] Number of compositions that returned storage pressures for each f_{O2}. Note that the averages of P_3 QFO and P_3 QFM include the P_4 QFOM pressures in the average and standard deviation calculations since the P_4 pressure will also return a P_3 pressure.

(A) Mean pressure calculation (MPa) and depth (km) [1]

	-3 ΔNNO	**-2.5 ΔNNO**	**-2 ΔNNO**	**-1.5 ΔNNO**	**-1 ΔNNO**	**-0.5 ΔNNO**	**0 ΔNNO**
P_4 QFOM	-	-	-	-	50 MPa (1.9; 2.0 km)	41 MPa (1.6; 1.7 km)	-
P_3 QFO	36 MPa (1.4; 1.5 km)	40 MPa (1.5; 1.6 km)	41 MPa (1.6; 1.7 km)	45 MPa (1.7; 1.8 km)	48 MPa (1.8; 2.0 km)	91 MPa (3.4; 3.7 km)	126 MPa (4.8; 5.1 km)
P_3 QFM	-	-	-	-	51 MPa (1.9; 2.1 km)	34 MPa (1.3; 1.4 km)	17 MPa (0.6; 0.7 km)

(B) Standard deviation pressure calculation (MPa) and depth (km) [2]

P_4 QFOM	-	-	-	-	6 MPa (0.2; 0.3 km)	8 MPa (0.3; 0.4 km)	-
P_3 QFO	9 MPa (0.3; 0.4 km)	9 MPa (0.3; 0.4 km)	9 MPa (0.3; 0.4 km)	10 MPa (0.4; 0.4 km)	11 MPa (0.4; 0.5 km)	46 MPa (1.8; 1.9 km)	25 MPa (0.9; 1.0 km)
P_3 QFM	-	-	-	-	8 MPa (0.3; 0.3 km)	8 MPa (0.3; 0.3 km)	5 MPa (0.2; 0.2 km)

(C) Number of compositions that return pressures for each f_{O2}[3]

P_4 QFOM	0	0	0	0	20	7	0
P_3-QFO	51	66	60	68	32	10	3
P_3-QFM	0	0	0	0	5	42	9
Number of comps	85	83	90	102	72	74	94

Table 2. Pressure calculations for Monte Carlo compositions from Krafla average composition.

[1] Mean of P_4 QFOM, P_3 QFO, and P_3 QFM storage pressures for Monte Carlo Krafla RHL compositions for different f_{O2} reported in MPa and km; the densities used to convert pressure to depth are 2,700 kg/m^3 and 2,500 kg/m^3

[2] Standard deviation of P_4 QFOM, P_3 QFO, and P_3 QFM storage pressures for Monte Carlo Krafla RHL compositions reported in MPa and km

[3] Number of compositions that returned storage pressures for each f_{O2}. Note that the averages of P_3 QFO and P_3 QFM include the P_4 QFOM pressures in the average, standard deviation calculations since the P_4 pressure will also return a P_3 pressure.